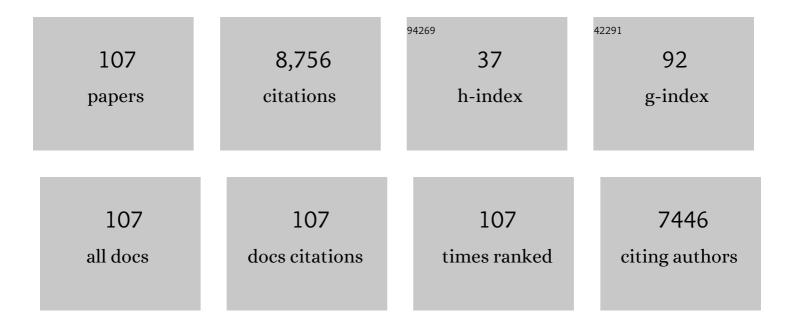
## Mohamedally Kurmoo

List of Publications by Year in descending order

Source: https://exaly.com/author-pdf/4887966/publications.pdf Version: 2024-02-01



#	Article	IF	CITATIONS
1	Magnetic metal–organic frameworks. Chemical Society Reviews, 2009, 38, 1353.	18.7	2,304
2	Rigid Pillars and Double Walls in a Porous Metal-Organic Framework: Single-Crystal to Single-Crystal, Controlled Uptake and Release of Iodine and Electrical Conductivity. Journal of the American Chemical Society, 2010, 132, 2561-2563.	6.6	620
3	Superconducting and Semiconducting Magnetic Charge Transfer Salts: (BEDT-TTF)4AFe(C2O4)3.cntdot.C6H5CN (A = H2O, K, NH4). Journal of the American Chemical Society, 1995, 117, 12209-12217.	6.6	578
4	Recent advances in post-synthetic modification of metal–organic frameworks: New types and tandem reactions. Coordination Chemistry Reviews, 2019, 378, 500-512.	9.5	428
5	Nanoporous Cobalt(II) MOF Exhibiting Four Magnetic Ground States and Changes in Gas Sorption upon Post-Synthetic Modification. Journal of the American Chemical Society, 2014, 136, 4680-4688.	6.6	387
6	The concept of mixed organic ligands in metal–organic frameworks: design, tuning and functions. Dalton Transactions, 2015, 44, 5258-5275.	1.6	225
7	Layered Cobalt Hydroxysulfates with Both Rigid and Flexible Organic Pillars:  Synthesis, Structure, Porosity, and Cooperative Magnetism. Journal of the American Chemical Society, 2001, 123, 10584-10594.	6.6	207
8	Hierarchical Assembly of a {Mn <sup>II</sup> <sub>15</sub> Mn <sup>III</sup> <sub>4</sub> } Brucite Disc: Step-by-Step Formation and Ferrimagnetism. Journal of the American Chemical Society, 2016, 138, 1328-1334.	6.6	179
9	Tracking the Formation of a Polynuclear Co <sub>16</sub> Complex and Its Elimination and Substitution Reactions by Mass Spectroscopy and Crystallography. Journal of the American Chemical Society, 2013, 135, 7901-7908.	6.6	162
10	Electrochromic two-dimensional covalent organic framework with a reversible dark-to-transparent switch. Nature Communications, 2020, 11, 5534.	5.8	149
11	Two Modifications of Layered Cobaltous Terephthalate: Crystal Structures and Magnetic Properties. Journal of Solid State Chemistry, 2001, 159, 343-351.	1.4	137
12	Tandem Postsynthetic Modification of a Metal–Organic Framework by Thermal Elimination and Subsequent Bromination: Effects on Absorption Properties and Photoluminescence. Angewandte Chemie - International Edition, 2013, 52, 4538-4543.	7.2	131
13	Trapping an octahedral Ag6 kernel in a seven-fold symmetric Ag56 nanowheel. Nature Communications, 2018, 9, 2094.	5.8	129
14	Hard Magnets Based on Layered Cobalt Hydroxide:  The Importance of Dipolar Interaction for Long-Range Magnetic Ordering. Chemistry of Materials, 1999, 11, 3370-3378.	3.2	128
15	Different Silver Nanoparticles in One Crystal: Ag <sub>210</sub> ( <sup><i>i</i></sup> PrPhS) <sub>71</sub> (Ph <sub>3</sub> P) <sub>5</sub> Cl and Ag <sub>211</sub> ( <sup><i>i<i< i=""></i<></i></sup> PrPhS) <sub>71</sub> (Ph <sub>3</sub> P) <sub>6</sub> Cl. Angewandte Chemie - International Edition, 2019, 58, 195-199.	7.2	118
16	Hydrogen-Bonded Dicubane Co <sup>II</sup> <sub>7</sub> Single-Molecule-Magnet Coordinated by in Situ Solvothermally Generated 1,2-Bis(8-hydroxyquinolin-2-yl)ethane-1,2-diol Arranged in a Trefoil. Chemistry of Materials, 2010, 22, 2114-2119.	3.2	115
17	A Twoâ€Dimensional Iron(II) Coordination Polymer with Synergetic Spinâ€Crossover and Luminescent Properties. Angewandte Chemie - International Edition, 2019, 58, 8789-8793.	7.2	115
18	A Porous 4-Fold-Interpenetrated Chiral Framework Exhibiting Vapochromism, Single-Crystal-to-Single-Crystal Solvent Exchange, Gas Sorption, and a Poisoning Effect. Inorganic Chemistry, 2013, 52, 2353-2360.	1.9	114

#	Article	IF	CITATIONS
19	Solventâ€Controlled Phase Transition of a Co <sup>II</sup> â€Organic Framework: From Achiral to Chiral and Two to Three Dimensions. Chemistry - A European Journal, 2017, 23, 7990-7996.	1.7	111
20	Traditional and Microwave-Assisted Solvothermal Synthesis and Surface Modification of Co <sub>7</sub> Brucite Disk Clusters and Their Magnetic Properties. Chemistry of Materials, 2010, 22, 4295-4303.	3.2	107
21	Core–Shell {Mn7âŠ,(Mn,Cd)12} Assembled from Core {Mn7} Disc. Journal of the American Chemical Society, 2017, 139, 14033-14036.	6.6	98
22	Reversible SCâ€SC Transformation involving [4+4] Cycloaddition of Anthracene: A Singleâ€lon to Singleâ€Molecule Magnet and Yellowâ€Green to Blueâ€White Emission. Angewandte Chemie - International Edition, 2018, 57, 8577-8581.	7.2	97
23	Field-Induced Ferrimagnetic State in a Molecule-Based Magnet Consisting of a Co <sup>II</sup> Ion and a Chiral Triplet Bis(nitroxide) Radical. Journal of the American Chemical Society, 2007, 129, 9902-9909.	6.6	95
24	Assembly of a Highly Stable Luminescent Zn <sub>5</sub> Cluster and Application to Bioâ€Imaging. Angewandte Chemie - International Edition, 2016, 55, 11407-11411.	7.2	88
25	A Metal–Organic Framework Based on a Nickel Bis(dithiolene) Connector: Synthesis, Crystal Structure, and Application as an Electrochemical Glucose Sensor. Journal of the American Chemical Society, 2020, 142, 20313-20317.	6.6	83
26	A Multifaceted Cage Cluster, [Co <sup>II</sup> <sub>6</sub> O <sub>12</sub> ⊃ X] <sup>â^'</sup> (X =) Tj E Materials, 2010, 22, 4328-4334.	TQq0 0 0 1 3.2	rgBT /Overloc 78
27	Chalcogens-Induced Ag <sub>6</sub> Z <sub>4</sub> @Ag <sub>36</sub> (Z = S or Se) Core–Shell Nanoclusters: Enlarged Tetrahedral Core and Homochiral Crystallization. Journal of the American Chemical Society, 2019, 141, 17884-17890.	6.6	76
28	Anion-templated nanosized silver clusters protected by mixed thiolate and diphosphine. Nanoscale, 2017, 9, 3601-3608.	2.8	71
29	Redox Activities of Metal–Organic Frameworks Incorporating Rare-Earth Metal Chains and Tetrathiafulvalene Linkers. Inorganic Chemistry, 2019, 58, 3698-3706.	1.9	66
30	A Water-Stable Cl@Ag <sub>14</sub> Cluster Based Metal–Organic Open Framework for Dichromate Trapping and Bacterial Inhibition. Inorganic Chemistry, 2017, 56, 11891-11899.	1.9	60
31	Nuclear and Magnetic Structures and Magnetic Properties of the Layered Cobalt Hydroxysulfate Co5(OH)6(SO4)2(H2O)4and Its Deuterated Analogue, Co5(OD)6(SO4)2(D2O)4. Journal of the American Chemical Society, 2006, 128, 7972-7981.	6.6	54
32	Microwave versus Traditional Solvothermal Synthesis of Ni <sub>7</sub> <sup>II</sup> Discs: Effect of Ligand on Exchange Reaction in Solution Studied by Electrospray Ionization-Mass Spectroscopy and Magnetic Properties. Inorganic Chemistry, 2011, 50, 7274-7283.	1.9	51
33	General Assembly of Twisted Trigonalâ€Prismatic Nonanuclear Silver(I) Clusters. Chemistry - A European Journal, 2016, 22, 3019-3028.	1.7	47
34	In Situ Pyrolysis Tracking and Realâ€Time Phase Evolution: From a Binary Zinc Cluster to Supercapacitive Porous Carbon. Angewandte Chemie - International Edition, 2020, 59, 13232-13237.	7.2	44
35	Coupling photo-, mechano- and thermochromism and single-ion-magnetism of two mononuclear dysprosium–anthracene–phosphonate complexes. Chemical Communications, 2018, 54, 3278-3281.	2.2	39
36	Concomitant Use of Tetrathiafulvalene and 7,7,8,8-Tetracyanoquinodimethane within the Skeletons of Metal–Organic Frameworks: Structures, Magnetism, and Electrochemistry. Inorganic Chemistry, 2019, 58, 8657-8664.	1.9	39

#	Article	IF	CITATIONS
37	Ruthenium-Catalyzed Gram-Scale Preferential C–H Arylation of Tertiary Phosphine. Organic Letters, 2019, 21, 2885-2889.	2.4	39
38	Stepwise Assembly of M <sup>II</sup> <sub>7</sub> Clusters Revealed by Mass Spectrometry, EXAFS, and Crystallography. Chemistry - A European Journal, 2016, 22, 18404-18411.	1.7	38
39	Structure, solution assembly, and electroconductivity of nanosized argento-organic-cluster/framework templated by chromate. Nanoscale, 2017, 9, 5305-5314.	2.8	38
40	Canted Antiferromagnetism in an Organo-modified Layered Nickel Phyllosilicate. Chemistry of Materials, 2002, 14, 3829-3836.	3.2	37
41	Near-Infrared Emitters: Stepwise Assembly of Two Heteropolynuclear Clusters with Tunable Ag <sup>I</sup> :Zn <sup>II</sup> Ratio. Inorganic Chemistry, 2016, 55, 4757-4763.	1.9	35
42	Different Silver Nanoparticles in One Crystal: Ag <sub>210</sub> ( <sup><i>i</i>/i&gt;</sup> PrPhS) <sub>71</sub> (Ph <sub>3</sub> P) <sub>5</sub> Cl and Ag <sub>211</sub> ( <sup><i>i</i>/i&gt;</sup> PrPhS) <sub>71</sub> (Ph <sub>3</sub> P) <sub>6</sub> Cl. Angewandte Chemie, 2019, 131, 201-205.	1.6	34
43	Exploring the Effect of Metal Ions and Counteranions on the Structure and Magnetic Properties of Five Dodecanuclear Co <sup>II</sup> and Ni <sup>II</sup> Clusters. Chemistry - A European Journal, 2011, 17, 14084-14093.	1.7	33
44	Ligand Effect on the Single-Molecule Magnetism of Tetranuclear Co(II) Cubane. Inorganic Chemistry, 2017, 56, 15178-15186.	1.9	33
45	Manipulating Clusters by Use of Competing N,Oâ€Chelating Ligands: A Combined Crystallographic, Mass Spectrometric, and DFT Study. Chemistry - A European Journal, 2018, 24, 7906-7912.	1.7	33
46	Precise Implantation of an Archimedean Ag@Cu <sub>12</sub> Cuboctahedron into a Platonic Cu <sub>4</sub> Bis(diphenylphosphino)hexane <sub>6</sub> Tetrahedron. ACS Nano, 2021, 15, 8733-8741.	7.3	33
47	Enhanced dielectricity coupled to spin-crossover in a one-dimensional polymer iron(ii) incorporating tetrathiafulvalene. Chemical Science, 2020, 11, 6229-6235.	3.7	32
48	Microwave and traditional solvothermal syntheses, crystal structures, mass spectrometry and magnetic properties of Coll4O4 cubes. Dalton Transactions, 2013, 42, 5439.	1.6	30
49	Hierarchical Assembly and Aggregation-Induced Enhanced Emission of a Pair of Isostructural Zn <sub>14</sub> Clusters. Inorganic Chemistry, 2017, 56, 14069-14076.	1.9	29
50	Tuning Electrical―and Photoâ€Conductivity by Cation Exchange within a Redoxâ€Active Tetrathiafulvaleneâ€Based Metal–Organic Framework. Angewandte Chemie - International Edition, 2020, 59, 18763-18767.	7.2	29
51	Three Properties in One Coordination Complex: Chirality, Spin Crossover, and Dielectric Switching. European Journal of Inorganic Chemistry, 2017, 2017, 3144-3149.	1.0	29
52	Late-Stage Modification of Tertiary Phosphines via Ruthenium(II)-Catalyzed C–H Alkylation. Organic Letters, 2020, 22, 1331-1335.	2.4	28
53	Biomimetic Transformation by a Crystal of a Chiral Mn <sup>II</sup> –Cr <sup>III</sup> Ferrimagnetic Prussian Blue Analogue. Chemistry of Materials, 2016, 28, 7029-7038.	3.2	25
54	A Porous Metal–Organic Framework [Zn <sub>2</sub> (bdc)( <scp>l</scp> -lac)] as a Coating Material for Capillary Columns of Gas Chromatography. Inorganic Chemistry, 2017, 56, 11043-11049.	1.9	25

#	Article	IF	CITATIONS
55	Magnetic Properties and Magnetic Structures of Synthetic Natrochalcites, NaMII2(D3O2)(MoO4)2, M = Co or Ni. Journal of the American Chemical Society, 2008, 130, 13490-13499.	6.6	24
56	Iterative Mass Spectrometry and X-Ray Crystallography to Study Ion-Trapping and Rearrangements by a Flexible Cluster. Scientific Reports, 2013, 3, 3516.	1.6	24
57	Interplay of anthracene luminescence and dysprosium magnetism by steric control of photodimerization. Dalton Transactions, 2019, 48, 13769-13779.	1.6	24
58	Tuning Electrical―and Photoâ€Conductivity by Cation Exchange within a Redoxâ€Active Tetrathiafulvaleneâ€Based Metal–Organic Framework. Angewandte Chemie, 2020, 132, 18922-18926.	1.6	24
59	Hierarchical tandem assembly of planar [3×3] building units into {3×[3×3]} oligomers: mixed-valency, electrical conductivity and magnetism. Chemical Science, 2018, 9, 7498-7504.	3.7	23
60	Luminescent Ir( <scp>iii</scp> )–Ln( <scp>iii</scp> ) coordination polymers showing slow magnetization relaxation. Inorganic Chemistry Frontiers, 2020, 7, 4580-4592.	3.0	23
61	Discrete Heteropolynuclear Yb/Er Assemblies: Switching on Molecular Upconversion Under Mild Conditions. Angewandte Chemie - International Edition, 2021, 60, 22368-22375.	7.2	23
62	Carboxylate-Assisted Pd(II)-Catalyzed <i>ortho</i> -C–H and Remote C–H Activation: Economical Synthesis of Pyrano[4,3- <i>b</i> ]Indol-1(5 <i>H</i> )-ones. Organic Letters, 2019, 21, 2847-2850.	2.4	22
63	Self-Organization into Preferred Sites by Mg <sup>II</sup> , Mn <sup>II</sup> , and Mn <sup>III</sup> in Brucite-Structured M <sub>19</sub> Cluster. Inorganic Chemistry, 2019, 58, 3800-3806.	1.9	21
64	Rareâ€Earth Metal Tetrathiafulvalene Carboxylate Frameworks as Redoxâ€Switchable Singleâ€Molecule Magnets. Chemistry - A European Journal, 2021, 27, 622-627.	1.7	21
65	Chemical reaction within a compact non-porous crystal containing molecular clusters without the loss of crystallinity. Chemical Science, 2017, 8, 5356-5361.	3.7	20
66	Tracking the multiple-step formation of an iron(III) complex and its application in photodynamic therapy for breast cancer. Science China Chemistry, 2019, 62, 719-726.	4.2	20
67	Heptanuclear brucite disk with cyanide bridges in a cocrystal and tracking its pyrolysis to an efficient oxygen evolution electrode. Science Bulletin, 2019, 64, 1667-1674.	4.3	19
68	Metal–Metalloligand Coordination Polymer Embedding Triangular Cobalt–Oxo Clusters: Solvent- and Temperature-Induced Crystal to Crystal Transformations and Associated Magnetism. Inorganic Chemistry, 2020, 59, 8935-8945.	1.9	19
69	Ferromagnetic coupling in copper benzimidazole chloride: structural, mass spectrometry, magnetism, and DFT studies. Dalton Transactions, 2017, 46, 16663-16670.	1.6	18
70	Tracking the Progress and Mechanism Study of a Solvothermal in Situ Domino N-Alkylation Reaction of Triethylamine and Ammonia Assisted by Ferrous Sulfate. Inorganic Chemistry, 2017, 56, 10123-10126.	1.9	17
71	Field-induced slow magnetic relaxation in low-spin <i>S</i> = 1/2 mononuclear osmium( <scp>v</scp> ) complexes. Dalton Transactions, 2020, 49, 4084-4092.	1.6	16
72	Supramolecular Interactions Direct the Formation of Two Structural Polymorphs from One Building Unit in a Oneâ€Pot Synthesis. Chemistry - A European Journal, 2016, 22, 13900-13907.	1.7	15

#	Article	IF	CITATIONS
73	Two- and Three-Dimensional Heterometallic Ln[Ru2-α-Ammonium Diphosphonate] Nets: Structures, Porosity, Magnetism, and Proton Conductivity. Inorganic Chemistry, 2019, 58, 14034-14045.	1.9	15
74	A Chiral and Polar Single-Molecule Magnet: Synthesis, Structure, and Tracking of Its Formation Using Mass Spectrometry. Inorganic Chemistry, 2019, 58, 7236-7242.	1.9	15
75	From a layered iridium( <scp>iii</scp> )–cobalt( <scp>ii</scp> ) organophosphonate to an efficient oxygen-evolution-reaction electrocatalyst. Chemical Communications, 2019, 55, 13920-13923.	2.2	15
76	Hexadecanuclear Mn <sup>II</sup> <sub>2</sub> Mn <sup>III</sup> <sub>14</sub> Molecular Torus Built from <i>in Situ</i> Tandem Ligand Transformations. Inorganic Chemistry, 2019, 58, 14331-14337.	1.9	14
77	Copper(II)-Assisted Ligand Fragmentation Leading to Three Families of Metallamacrocycle. Inorganic Chemistry, 2020, 59, 13524-13532.	1.9	14
78	Co-Crystallization of Achiral Components into Chiral Network by Supramolecular Interactions: Coordination Complexes – Organic Radical. Crystal Growth and Design, 2017, 17, 4893-4899.	1.4	13
79	Progressive Structure Designing and Property Tuning of Manganese(II) Coordination Polymers with the Tetra(4-pyridyl)-tetrathiafulvalene Ligand. Crystal Growth and Design, 2019, 19, 3012-3018.	1.4	13
80	Fabrication of a capillary column coated with the four-fold-interpenetrated MOF Cd(D-Cam)(tmdpy) for gas chromatographic separation. Inorganic Chemistry Communication, 2017, 83, 123-126.	1.8	12
81	A rod-spacer mixed ligands MOF [Mn 3 (HCOO) 2 ( D -cam) 2 (DMF) 2 ] n as coating material for gas chromatography capillary column. Inorganic Chemistry Communication, 2017, 82, 34-38.	1.8	12
82	In-situ evolution process understanding from a salan-ligated manganese cluster to supercapacitive application. Nano Research, 2022, 15, 346.	5.8	12
83	A Cuprous [4 × 4] Grid: Single-Crystal to Single-Crystal Transformation and Fading of Luminescence by Solvent Inclusion. Inorganic Chemistry, 2018, 57, 15040-15043.	1.9	11
84	Remote and Selective C(sp <sup>2</sup> )–H Olefination for Sequential Regioselective Linkage of Phenanthrenes. Organic Letters, 2020, 22, 4129-4134.	2.4	11
85	Electrical Conductivity of Copper Hexamers Tuned by their Ground-State Valences. Inorganic Chemistry, 2018, 57, 3443-3450.	1.9	10
86	Incorporating Paramagnetic Ir <sup>IV</sup> Cl <sub>6</sub> <sup>2–</sup> in H-Bonded Networks of Metal-Phosphonate Hydrate: Slow Magnetic Relaxation and Proton Conduction. Crystal Growth and Design, 2019, 19, 4836-4843.	1.4	10
87	In Situ Metalâ€Assisted Ligand Modification Induces Mn 4 Clusterâ€toâ€Cluster Transformation: A Crystallography, Mass Spectrometry, and DFT Study. Chemistry - A European Journal, 2020, 26, 721-728.	1.7	9
88	Progressive Transformation between Two Magnetic Ground States for One Crystal Structure of a Chiral Molecular Magnet. Inorganic Chemistry, 2016, 55, 3047-3057.	1.9	8
89	Thermally Induced trans â€ŧo―cis Isomerization and Its Photoinduced Reversal Monitored using Absorption and Luminescence: Cooperative Effect of Metal Coordination and Steric Substituent. Chemistry - A European Journal, 2019, 25, 5177-5185.	1.7	8
90	Carbon Dioxide (CO <sub>2</sub> ) Fixation: Linearly Bridged Zn <sub>2</sub> Paddlewheel Nodes by CO <sub>2</sub> in a Metal–Organic Framework. Inorganic Chemistry, 2019, 58, 16040-16046.	1.9	7

#	Article	IF	CITATIONS
91	Difference in the Formation of Two Structural Types of V-Shaped M <sup>II</sup> <sub>3</sub> Clusters: Diffraction, Mass Spectrometry, and Magnetism. Inorganic Chemistry, 2019, 58, 7472-7479.	1.9	7
92	Design, structure and luminescent properties of a novel two-dimensional Cd(II) coordination polymer constructed from in situ generated 1-methyl-2-(3H-[1–3]triazol-4-yl)-1H-benzoimidazole. Inorganic Chemistry Communication, 2014, 43, 78-80.	1.8	6
93	In Situ Pyrolysis Tracking and Realâ€Time Phase Evolution: From a Binary Zinc Cluster to Supercapacitive Porous Carbon. Angewandte Chemie, 2020, 132, 13334-13339.	1.6	6
94	Silica–Organometallic One-Dimensional Hybrid Employing a Agâ^'i€ <sub>Câ•€</sub> Bond Connecting Alternating Ag <sub>4</sub> (NO <sub>3</sub> ) <sub>4</sub> and OctavinyIsilsesquioxane. Inorganic Chemistry, 2021, 60, 2899-2904.	1.9	6
95	Regulating structural dimensionality and emission colors by organic conjugation between Sm <sup>III</sup> at a fixed distance. Dalton Transactions, 2018, 47, 6908-6916.	1.6	5
96	A Domino Fusion of an Organic Ligand Depended on Metalâ€Induced and Oxygen Insertion, Unraveled by Crystallography, Mass Spectrometry, and DFT Calculations. Chemistry - A European Journal, 2021, 27, 2875-2881.	1.7	5
97	Iron(II) Spin Crossover Coordination Polymers Derived From a Redox Active Equatorial Tetrathiafulvalene Schiff-Base Ligand. Frontiers in Chemistry, 2021, 9, 692939.	1.8	5
98	Discrete Heteropolynuclear Yb/Er Assemblies: Switching on Molecular Upconversion Under Mild Conditions. Angewandte Chemie, 2021, 133, 22542-22549.	1.6	5
99	Sensitized near infrared emission through supramolecular d → f energy transfer within an ionic Ru( <scp>ii</scp> )–Er( <scp>iii</scp> ) pair. Dalton Transactions, 2018, 47, 2073-2078.	1.6	4
100	Monitoring fragmentation and oligomerization of a di-μ-methoxo bridged copper( <scp>ii</scp> ) complex: structure, mass spectrometry, magnetism and DFT studies. Dalton Transactions, 2019, 48, 13094-13100.	1.6	4
101	Retention of a Four-Fold Interpenetrating Cadmium–Organic Framework through a Three-Step Single Crystal Transformation. Inorganic Chemistry, 2021, 60, 8331-8338.	1.9	4
102	Engineering Heteronuclear Arrays from <scp>Ir<sup>III</sup>â€Metalloligand</scp> and <scp>Co<sup>II</sup></scp> Showing Coexistence of Slow Magnetization Relaxation and Photoluminescence. Chinese Journal of Chemistry, 2022, 40, 931-938.	2.6	4
103	Metal Site Segregation in Chair-Shaped MII4 Cluster: Crystallography, Mass Spectrometry, and Magnetic and Optical Properties. Crystal Growth and Design, 2019, 19, 7067-7076.	1.4	1
104	Fragmentation of a One-Dimensional Zinc Coordination Polymer and Partial Reassembly Evidenced by Mass Spectrometry. Crystal Growth and Design, 2019, 19, 6801-6805.	1.4	1
105	The dominance of sulfate over two organic ligands in the solvothermal assembly of an undecanuclear cobaltous cluster: crystallography and mass spectrometry. Dalton Transactions, 2020, 49, 17683-17688.	1.6	1
106	Frontispiece: In Situ Pyrolysis Tracking and Realâ€Time Phase Evolution: From a Binary Zinc Cluster to Supercapacitive Porous Carbon. Angewandte Chemie - International Edition, 2020, 59, .	7.2	0
107	Frontispiz: In Situ Pyrolysis Tracking and Realâ€Time Phase Evolution: From a Binary Zinc Cluster to Supercapacitive Porous Carbon. Angewandte Chemie, 2020, 132, .	1.6	Ο